Co-Crosslinked Water-Soluble Biopolymers as a Binder for High-Voltage $LiNi_{0.5}Mn_{1.5}O_4$ | Graphite Lithium-Ion Full Cells

Matthias Kuenzel,[a, b] Hyeongseon Choi,[a, b] Fanglin Wu,[a, b] Arefeh Kazzazi,[a, b] Peter Axmann,[c] Margret Wohlfahrt-Mehrens,[a, c] Dominic Bresser,*[a, b] and Stefano Passerini*[a, b]

The use of water-soluble, abundant biopolymers as binders for lithium-ion positive electrodes is explored because it represents a great step forward towards environmentally benign battery processing. However, to date, most studies that employ, for instance, carboxymethyl cellulose (CMC) as a binder have focused on rather low electrode areal loadings with limited relevance for industrial needs. This study concerns the use of natural guar gum (GG) as a binding agent for cobalt-free, high-voltage $LiNi_{0.5}Mn_{1.5}O_4$ (LNMO), which realizes electrodes with substantially increased areal loadings, low binder content, and greatly enhanced cycling stability. Co-crosslinking GG through citric acid with CMC allows for an enhanced rate capability and essentially maintains the beneficial impact of using GG as a binder rather than CMC only. Lithium-ion full cells based on water-processed LNMO and graphite electrodes provide a remarkably high cycling stability with 80% capacity retention after 1000 cycles at 1 C.

Introduction

After almost 30 years of lithium-ion battery (LIB) development, their performance metrics increasingly match the high requirements for application in electric vehicles (EVs). Therefore, car manufacturers around the world have initiated the mass-market introduction of EVs, which provide significantly lower CO_2 emissions than vehicles powered by the internal combustion engine (ICE).[1–6] To comply with the goal to reduce the environmental impact of the replacement of ICE vehicles with EVs, however, the sustainability of the LIB production itself needs to be considered as well.[7–10] This means that the use of scarce and toxic cobalt, for instance, should be avoided.[11–14] Moreover, mutagenic and teratogenic polyvinylidene difluoride (PVdF),[15] commonly utilized as a binder for the cathode,[16] should be replaced, not least as it requires the use of toxic and hazardous *N*-methylpyrrolidone (NMP)[17–19] as a solvent. Additional benefits of the implementation of more sustainable electrode materials and processing beyond health and safety aspects arise from the potential cost savings, which can be achieved simply by employing water as the processing solvent and natural polymers as the binder.[10,20–22] Among such greener processes, the combined use of styrene butadiene rubber (SBR) and carboxymethyl cellulose (CMC) as the binder is certainly the most prominent representative[10] as it has been fully established for the production of graphite negative electrodes.[23,24] However, the pronounced sensitivity of cathode materials, such as Co-free $LiNi_{0.5}Mn_{1.5}O_4$ (LNMO), towards water has so far hindered the large-scale introduction of aqueous fabrication routes for lithium-ion positive electrodes.[25–27] In the case of high-voltage LNMO, the second great challenge towards the identification of new binders concerns their stability towards oxidation. SBR, for instance, is not sufficiently stable at such elevated potentials, which means that new (bio)polymers need to be identified to realize mechanically stable, high-mass-loading, high-voltage electrodes for LIBs.[10,23,28,29] Recently, it has been shown that the detrimental side effects of aqueous cathode processing, which especially include lithium leaching, aluminum current collector corrosion, and improvable adhesion of (high loading) electrode coating layers to the current collector,[30,31] can be mitigated by implementing suitable processing additives, such as phosphoric acid (PA)[32–36] and citric acid (CA),[33,37] and by modifying the current collector.[31,38] These strategies have effectively prevented corrosion of the aluminum current collector and have led to stabilized current collector–active material–electrolyte interfaces by forming a protec-

[a] Dr. M. Kuenzel, H. Choi, F. Wu, Dr. A. Kazzazi, Dr. M. Wohlfahrt-Mehrens, Dr. D. Bresser, Prof. Dr. S. Passerini
Helmholtz Institute Ulm (HIU)
Helmholtzstrasse 11, 89081 Ulm (Germany)
E-mail: dominic.bresser@kit.edu
stefano.passerini@kit.edu
[b] Dr. M. Kuenzel, H. Choi, F. Wu, Dr. A. Kazzazi, Dr. D. Bresser, Prof. Dr. S. Passerini
Karlsruhe Institute of Technology (KIT)
P.O. Box 3640, 76021 Karlsruhe (Germany)
[c] Dr. P. Axmann, Dr. M. Wohlfahrt-Mehrens
Zentrum für Sonnenenergie- und Wasserstoff-Forschung Baden-Württemberg (ZSW), Helmholtzstrasse 8, 89081 Ulm (Germany)
Supporting Information and the ORCID identification number(s) for the author(s) of this article can be found under: https://doi.org/10.1002/cssc.201903483.

tive metal phosphate layer on the active material surface as well as the current collector that allows an improved binder network that is tethered covalently to the carbon-coated aluminum current collector. As a result, these optimized electrodes provide very stable long-term electrochemical performance comparable or even superior to LNMO-based electrodes based on the standard PVdF binder.[38] Nonetheless, the achievement of commercially relevant areal loading electrodes remains a great challenge in spite of the rather high amount of binder (≈5 wt%). Towards this end, guar gum (GG), a naturally available galactomannan-based polysaccharide (repeated D-mannose units branched with glycosidic D-galactose side chains), has been identified recently as suitable alternative.[39,40] Applications so far include alternative anode materials that follow an alloying or conversion-type lithium storage mechanism[41–44] as well as cathode materials such as lithium nickel manganese cobalt oxide (NMC)[45] and its lithium-rich derivative.[46] The benefits of using GG are the good rheological slurry behavior, which provides electrodes with high mechanical stability and tensile strength,[41,47–49] little electrolyte swelling,[43,50] and the ability to coordinate (dissolved) cations through the O atoms in the galactose side chains.[42,51] As it serves as a scavenger for, for example, polysulfides formed as intermediates in sulfur cathodes[52,53] or dissolved manganese cations from cathodes such as $LiMn_2O_4$, GG reduces the detrimental effect on the anode.[54–57] Interestingly, the use of GG has not been reported for high-voltage LNMO to our knowledge.

In this study, the employment of natural GG as a water-soluble binder for LNMO cathodes in combination with suitable electrode processing additives and CA as a naturally available crosslinker was investigated. Such optimized electrode preparation allows for a substantial decrease in binder content compared to previous studies on CMC only[33] (i.e., from 5 wt% to only 3 wt%) and extremely stable cycling for more than 500 cycles without significant capacity loss and, at the same time, enables greatly elevated mass loadings. The subsequent incorporation of minor amounts of CMC further enhances the rate capability. Eventually, the suitability of the approach is demonstrated in high-energy LNMO|graphite lithium-ion cells with both electrodes obtained from aqueous processes.

Results and Discussion

CMC-based LNMO electrodes showed a satisfactory electrochemical performance in lithium cells upon the introduction of CA and PA as processing additives (together CP–CMC) as well as a coating on the carbon-coated aluminum current collectors for improved electrical contact and adhesion.[33,38] As a result, electrodes that contain 5 wt% CA-crosslinked CMC binder and subjected to a PA treatment during slurry preparation (CP–CMC-5%) exhibit a very stable cycling performance and retain a specific discharge capacity of 107 mA h g^{-1} after 400 cycles, which corresponds to a capacity retention of approximately 89% (Figure 1a). However, to comply with the rather strict industry requirements, binder contents of 3 wt% and less are required.[58,59] Accordingly, the binder content in the electrode was decreased stepwise (with an increase of the active material content) from 5 to 4 and 3 wt%. This has a significant to substantial effect on the cycling stability (Figure 1a). For LNMO electrodes that contain 4 wt% binder (CP–CMC-4%), the capacity retention after 400 cycles is merely 82% (i.e., 98 mA h g^{-1}), whereas it decreases to 65% for electrodes prepared with only 3 wt% binder (82 mA h g^{-1}; CP–CMC-3%). Without crosslinking the binder through CA (PA–CMC-3%) the cycle life is inferior, even though the active mass loadings were limited to relatively low values (≈5 mg cm^{-2}). Interestingly, a low binder content of only 3 wt%, in the case of CP–CMC-3% and PA–CMC-3%, has a beneficial effect on the initial capacity, which does not show the typical increase at the beginning. This finding further supports our previous assignment that such an increase is caused by the slow electrolyte wetting of the crosslinked binder that covers the active material particles.[33] With only 3 wt% binder, this effect is essentially absent. In addition, a reduction of the binder content has a positive effect on the dispersion of the LNMO particles and the conductive carbon, as revealed by the decreased tendency of these two components to form larger agglomerates with decreased binder contents (Figure 1b–d). Accordingly, the targeted decrease of the binder content promises to address the two issues (initial capacity increase and active material fraction) that so far hinder the commercial exploitation of aqueous electrode processing routes for high-energy cathodes. Nonetheless, the inferior cycling stability is also an important issue. An examination of the pristine electrodes by using SEM (Figure 1b–d) reveals that 3 wt% binder is not sufficient to obtain mechanically intact electrodes because of the rather brittle and stiff nature of CMC.[48,60] The large cracks in the coating layer of the pristine (Figure 1d) and cycled electrodes (Figure S1) provide an explanation for the pronounced capacity fading, which is at least partially related to the loss of active material or the electronic wiring in the electrode as indicated by the shortening of the voltage plateau (inset in Figure 1a).

A suitable alternative for CMC might be GG thanks to its high tensile strength and excellent flexibility,[41,47–49] which would potentially yield electrodes with a good mechanical stability. After our previous findings that demonstrated the advantages of CA-induced crosslinking,[33] we applied this approach to GG-based electrodes. The branched GG chains can also be crosslinked by CA according to the simple condensation reaction illustrated in Figure 2a. Specifically, the hydroxyl groups along the GG chain are expected to react with the carboxylic acid groups of CA by forming ester bonds accompanied by the release of water at slightly elevated temperatures of 150 °C.

The occurrence of this crosslinking reaction was confirmed by using FTIR spectroscopy (Figure 2b). For reference, the spectra of CA, GG, and a non-crosslinked mixture of CA and GG (1:9) are given. The latter, as expected, simply resembles the sum of the individual compounds. The spectrum obtained for the crosslinked film with the same CA:GG ratio reveals a new band at $\tilde{\nu}=1722\ cm^{-1}$, which is characteristic for the carbonyl stretching vibration in ester groups. This confirms the occurrence of the crosslinking esterification reaction between CA and GG, as reported previously for similar polymers, such

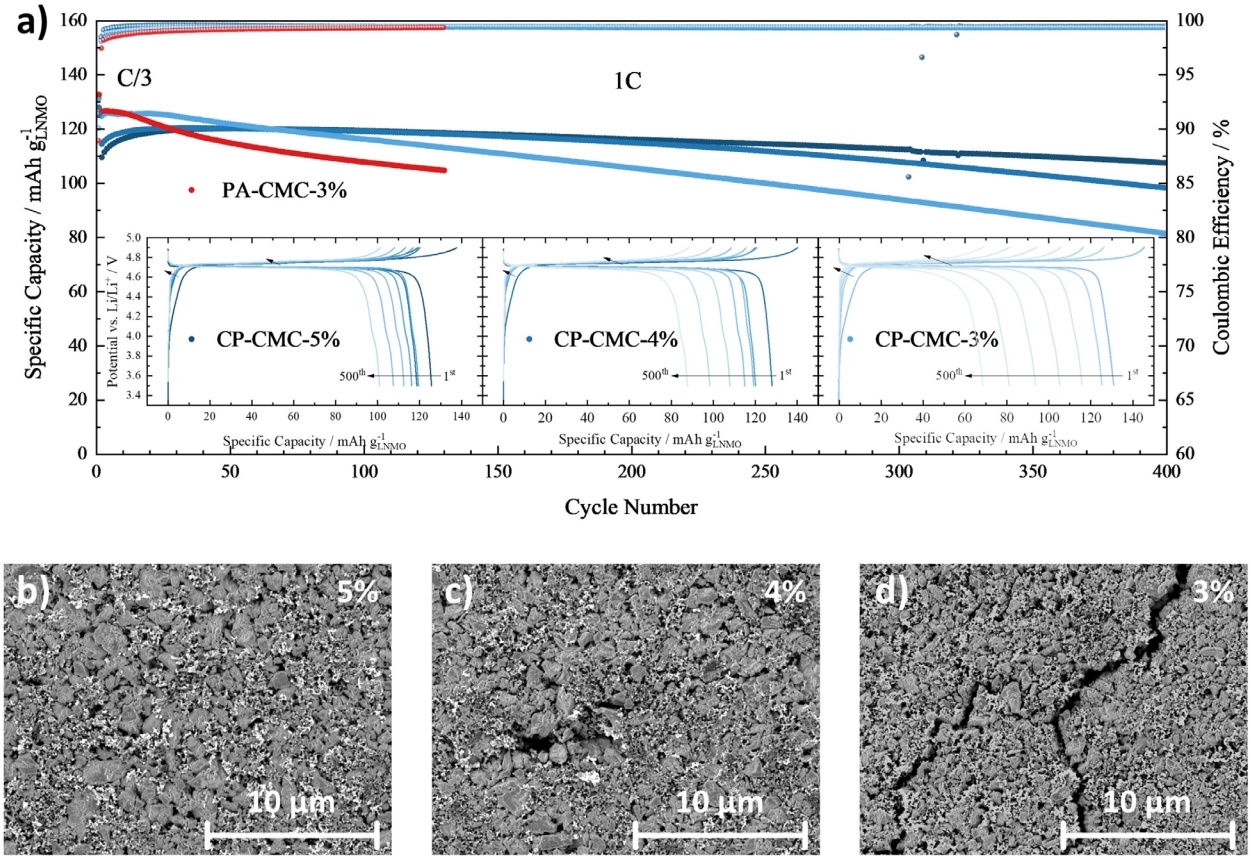

Figure 1. a) Extended constant current cycling of CA-crosslinked CP–CMC electrodes with different weight fractions of binder (5 wt% in dark blue, 4 wt% in blue, 3 wt% in light blue). The performance of the non-crosslinked PA–CMC (3 wt%) electrode is also presented (red) as a reference. Selected potential profiles for the three CP–CMC electrodes with 5, 4, and 3 wt% binder are also shown. The cut-off potentials were set to 3.5 and 4.9 V, and a charge–discharge rate of 1 C corresponds to a specific current of 147 mA g^{-1}. b–d) SEM images of pristine electrodes based on b) 5, c) 4, and d) 3 wt% CP CMC. All electrodes have an areal loading of approximately 5 mg cm^{-2}.

as CMC with CA, CMC with poly(acrylic acid) (PAA), or poly(vinyl alcohol) with PAA.[33,61–63] The other bands remain essentially unchanged compared to spectrum of the bare GG sample with broad features between $\tilde{\nu}=1250$ and 1650 cm^{-1} ascribed to the bending vibrations of C–H and O–H along the polysaccharide chain and/or associated water trapped in the binder film. Additionally, the symmetric ($\tilde{\nu}=1145$ cm^{-1}) and asymmetric ($\tilde{\nu}=868$ cm^{-1}) stretching vibrations of the ether bonds, which form the glycosidic linkages of the polysaccharide, as well as those in the mannose backbone ($\tilde{\nu}=$ 1015 cm^{-1}) are hardly affected by the crosslinking.[43,64–66] Only the intensities of the C–OH stretching vibration of primary alcohols at approximately $\tilde{\nu}=1058$ cm^{-1} decrease slightly, which indicates the consumption of the alcohol groups of GG in the formation of the ester bonds with CA. This finding is complemented by the shoulder between $\tilde{\nu}=1150$ and 1220 cm^{-1} that evolves into a more pronounced band, which corresponds to the stretching vibration of C–O–CO in carbonyl esters.[63]

The beneficial impact of such crosslinking for CP–GG-3% is reflected in the significantly increased long-term cycling stability compared to that of the non-crosslinked PA–GG-3% electrodes (Figure 3a). A comparison of the corresponding potential profiles (inset in Figure 3a) further highlights the performance improvement. Importantly, the cycling stability in general is enhanced dramatically if CMC is replaced by GG despite the rather low binder content (3 wt%). Even for the non-crosslinked GG-based electrodes, a capacity of 107 mA h g^{-1} is recorded after 400 cycles, which corresponds to a capacity retention of approximately 92%. This value is already higher than that of the best-performing CMC-based electrodes that have a capacity retention of approximately 89% at a higher binder content (5 wt%). For the crosslinked CP–GG-3% electrodes, the capacity retention is further improved to approximately 96% with a final specific capacity of more than 110 mA h g^{-1}. Moreover, with the use of the CA-crosslinked GG binder, a substantial increase in active material mass loading from approximately 3 to approximately 9 mg cm^{-2} is enabled without a significant loss of electrochemical performance at lower C-rates up to 1 C (Figure 3b).

However, the initial capacity increase, assigned to the wetting effect, becomes more pronounced at such high loadings. At high charge and discharge rates, the achieved discharge capacity, for example, at 5 C decreases by more than 50% if we compare the highest and lowest mass loadings, as the polarization increases substantially with an increase of the mass loading (Figure 3c). Nonetheless, if we return to relatively low

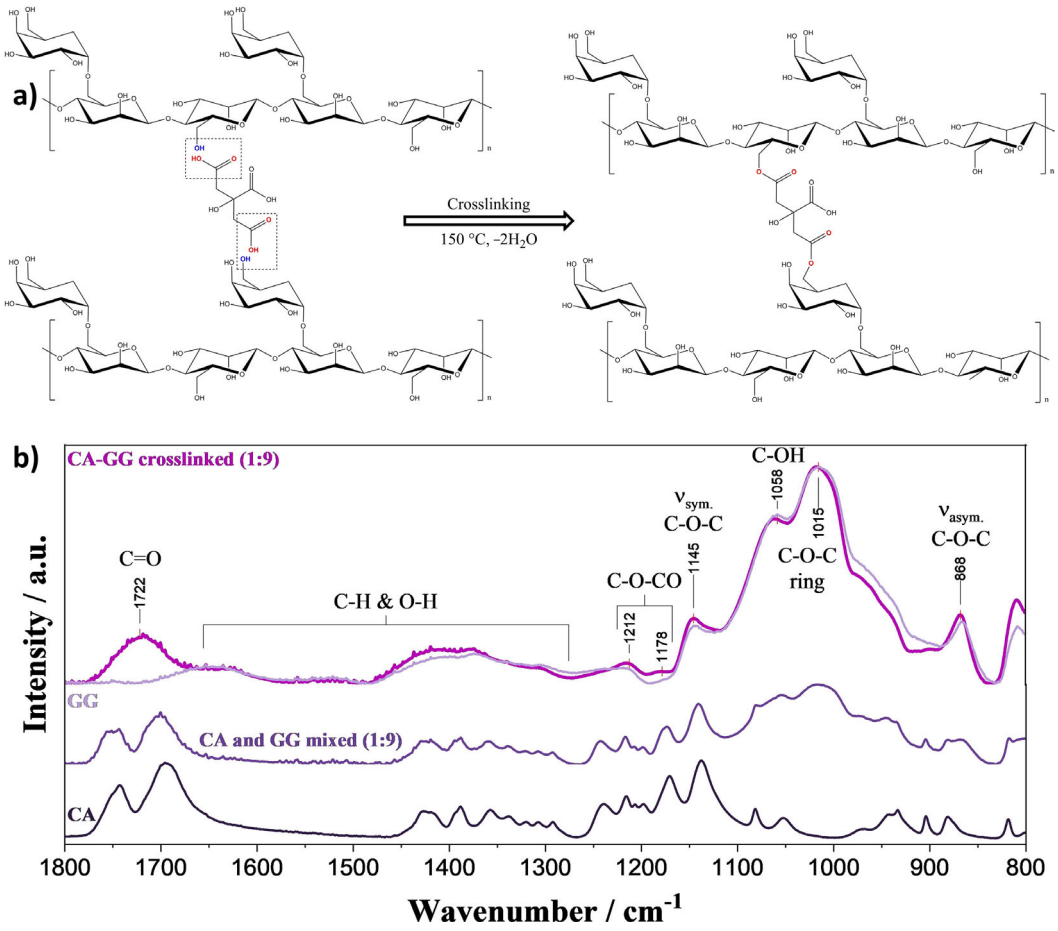

Figure 2. a) Proposed crosslinking through the temperature-induced ester condensation of free hydroxyl groups in the GG side chain and CA. b) FTIR spectra of CA (dark purple), the simple mixture of CA and GG without temperature treatment (CA+GG, purple), pure GG (light purple), and CA-crosslinked GG (CA–GG, pink) with the characteristic ester-related band at $\tilde{\nu} = 1722\ cm^{-1}$, which indicates the crosslinking reaction.

charge and discharge rates, that is, C/3, the capacity increases again to its initial value for all different mass loadings and remains stable above 120 mA h g^{-1} (Figure 3b). This superior electrochemical performance compared to that of the electrodes based on CMC only is ascribed to the ability of GG to coordinate to oxide-based active materials to form a rather stable (electrode) network, which thus enables increased active material mass loadings.[44] This beneficial behavior is further amplified by CA-induced crosslinking.[33,37,38] GG-based electrodes with increased mass loadings do not significantly differ in their appearance. They all display a densely packed but well-distributed mixture of conductive carbon and active material interconnected by thin binder strings (not shown here because of immediate beam damage) without any severe cracks in the coating layer and only very few large pores in the case of the thickest electrode (Figure 3d–f).

The impact of the binder and its content on the rate performance was investigated by fixing the electrode areal loading to approximately 5 mg cm^{-2} (Figure 4). The results are also compared with those of CMC-based electrodes with different binder contents. At lower C rates, there is no significant effect thanks to the initial "wetting cycle" at C/10, up to a charge and discharge rate of C/2 (Figure 4a). At elevated C rates, however, the CMC-based electrodes outperform CP–GG-3% clearly, and the lower the CMC content the higher the rate capability. This agrees with the better distribution of the LNMO active material and conductive carbon additive reported earlier, and the conductive carbon additive forms an improved percolating network throughout the electrode. However, the GG-based electrodes suffer a pronounced polarization if the specific current is increased (Figure 4b). This is attributed to the extended interaction of the insulating GG with the LNMO particle surface,[42,43,46,50] which provides, on one hand, better mechanical stability and electrode integrity but, on the other hand, limits the high rate performance of such electrodes because of a higher charge transfer resistance (Figure S2). Remarkably, the combination of the two binders CMC and GG (GG–X–CMC-3%) provides the same rate capability as electrodes that comprise CMC only (CP–CMC-3%) with only relatively little polarization (Figure 4a and b and Figure S2). If we compare the long-term cycling performance of the CMC-, GG-, and GG–X–CMC-based electrodes with 3 wt% binder, the cycling stability of the GG–X–CMC-based electrodes is only slightly inferior to that of the electrodes that employ only GG (Figure 4c) and they offer the best rate performance with a specific capacity above 120 mA h g^{-1} at 1 C.

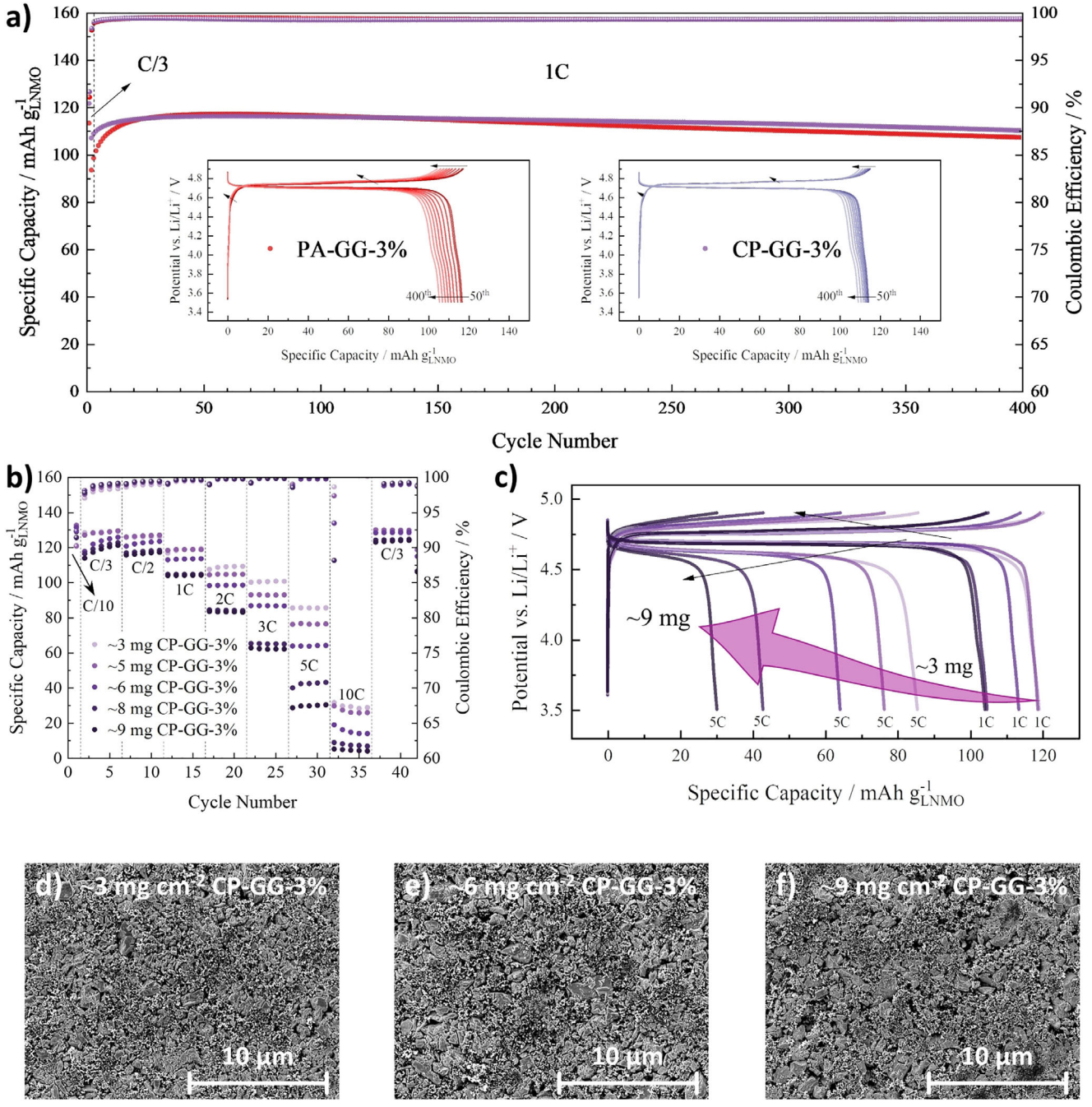

Figure 3. a) Specific capacity and selected potential profiles of electrodes that employ only 3 wt% GG as binder without (PA–GG, red) and with (CP–GG, purple) CA-induced crosslinking upon constant current cycling. b) Investigation of the rate capability for CP–GG electrodes with stepwise increased mass loadings from 3 (light purple) to 9 mg cm^{-2} (dark purple) and c) selected potential profiles for these electrodes at charge–discharge rates of 1 and 5 C. The cut-off potentials were set to 3.5 and 4.9 V, and a charge–discharge rate of 1 C corresponds to a specific current of 147 mA g^{-1}. d–f) SEM images of electrodes with d) low (3 mg cm^{-2}), e) intermediate (6 mg cm^{-2}), and f) high (9 mg cm^{-2}) areal loadings.

This superior performance is attributed to the formation of a co-crosslinked network of the two binders (Figure 5a). The CA molecules may interconnect the linear CMC molecules with the branched GG side chains through esterification to form a flexible binder network. Indeed, this is confirmed by the new band at approximately $\tilde{\nu}$ = 1720 cm^{-1} observed in the FTIR spectrum of GG–X–CMC (Figure 5b), which is characteristic for the C=O stretch in the carbonyl ester bond.[33,61–63] Once more, the crosslinking is induced by thermal treatment at 150 °C during the drying of the GG–CMC electrodes. Additionally, a new, rather broad band is also observed between $\tilde{\nu}$ = 1200 and 1250 cm^{-1} (which is absent in the spectrum of the simple mixture of the two polymers, CMC+GG) that can be ascribed to the stretching vibration of C–O–CO in carbonyl esters,[63] which further supports the proposed condensation-type crosslinking between the CMC and GG chains through CA. This is

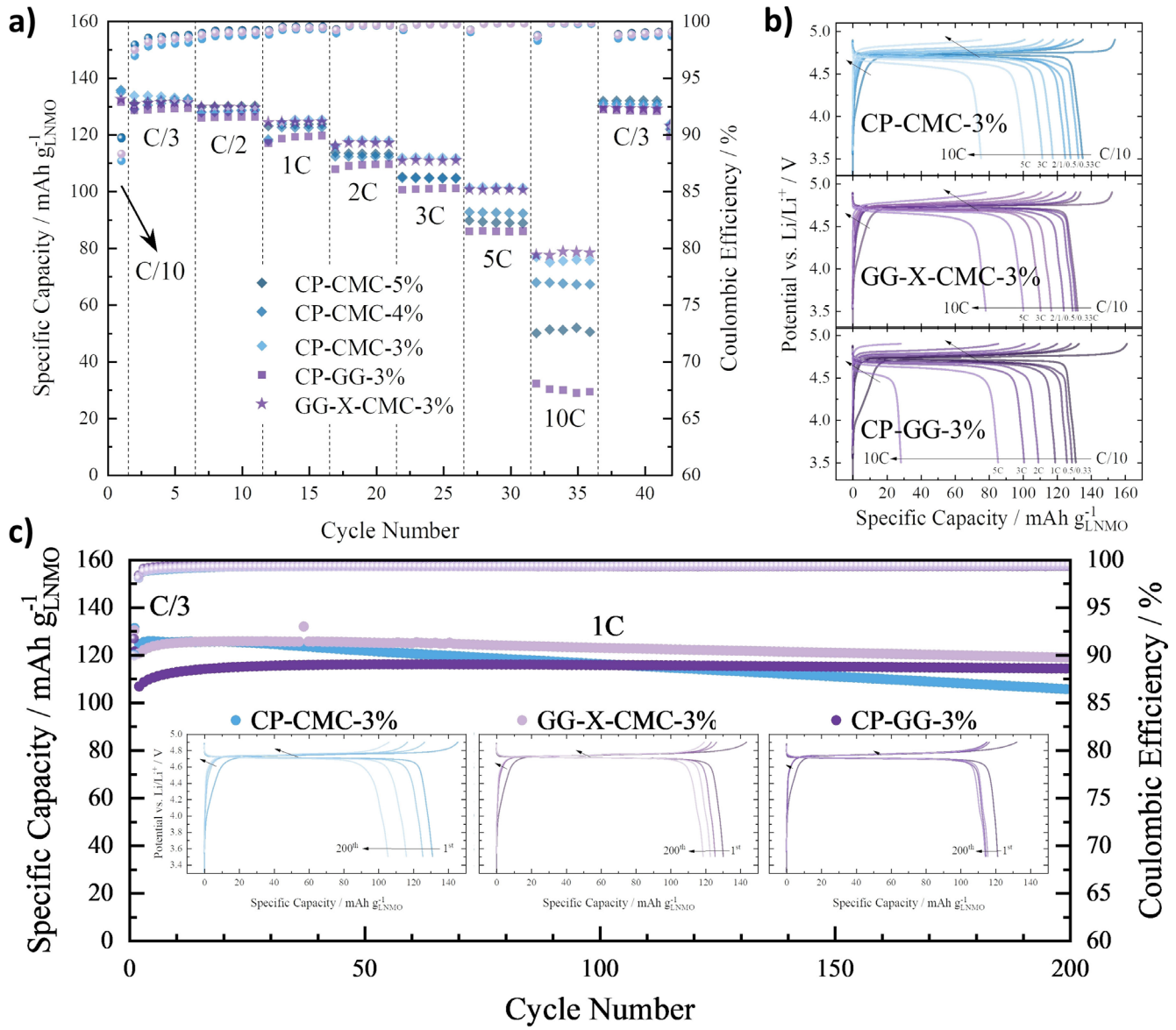

Figure 4. a) Rate capability of crosslinked CMC-based LNMO electrodes with different binder contents (5 wt% dark blue, 4 wt% blue, 3 wt% light blue, all CP–CMC) as well as electrodes based on 3 wt% CP–GG (dark purple) and the co-crosslinked blend of CMC and GG (3 wt%, GG–X–CMC) and b) selected potential profiles for the electrodes with only 3 wt% binder at various C rates. c) Constant current cycling of these electrodes with selected potential profiles over 200 cycles. The cut-off potentials were set to 3.5 and 4.9 V, and a charge–discharge rate of 1 C corresponds to a specific current of 147 mA g^{-1}. The compared electrodes have areal loading of approximately 5 mg cm^{-2}.

substantially different from the spectrum of the simple mixture of all three components (CMC+CA+GG, 1:1:1) given for reference that merely resembles the sum of the spectra recorded of the single materials (CA, GG, and CMC; Figure 5 b, bottom).

Similar to CP–GG electrodes, GG–X–CMC electrodes can achieve areal loadings that exceed 9 mg cm^{-2}, maintain high mechanical stability, and offer a remarkably improved rate capability up to 3 C. At such a high rate, the GG–X–CMC electrodes with an areal loading of 9 mg cm^{-2} still deliver 75% of their initial capacity at C/3 (i.e., 91 mA h g^{-1} compared to 121 mA h g^{-1} at C/3; Figure 6 a). At even higher C rates, however, the Ohmic drop and cell polarization increase significantly for the electrodes with areal loadings of 7 mg cm^{-2} and higher (Figure 6 b), which also affects the long-term cycling stability at 1 C (Figure 6 c and d). Although the electrodes with the lowest areal loading (3 mg cm^{-2}) display the most stable performance (i.e., specific capacity of 118 mA h g^{-1} after 200 cycles, which corresponds to 94% capacity retention) the electrodes with the highest mass loading (9 mg cm^{-2}) provide a specific capacity of 100 mA h g^{-1} in the 200th cycle, which corresponds to an 85% capacity retention. It appears reasonable to anticipate that the additional optimization of the binder ratio, the electrode composition, and the slurry and electrode processing (especially with respect to slurry mixing and coating as well as electrode calendaring) may, indeed, enable a further enhancement of the performance of the high-mass-loading electrodes.[59,67,68]

To further highlight the suitability of GG as a binder for LNMO-based cathodes and the viability of fully-water-based

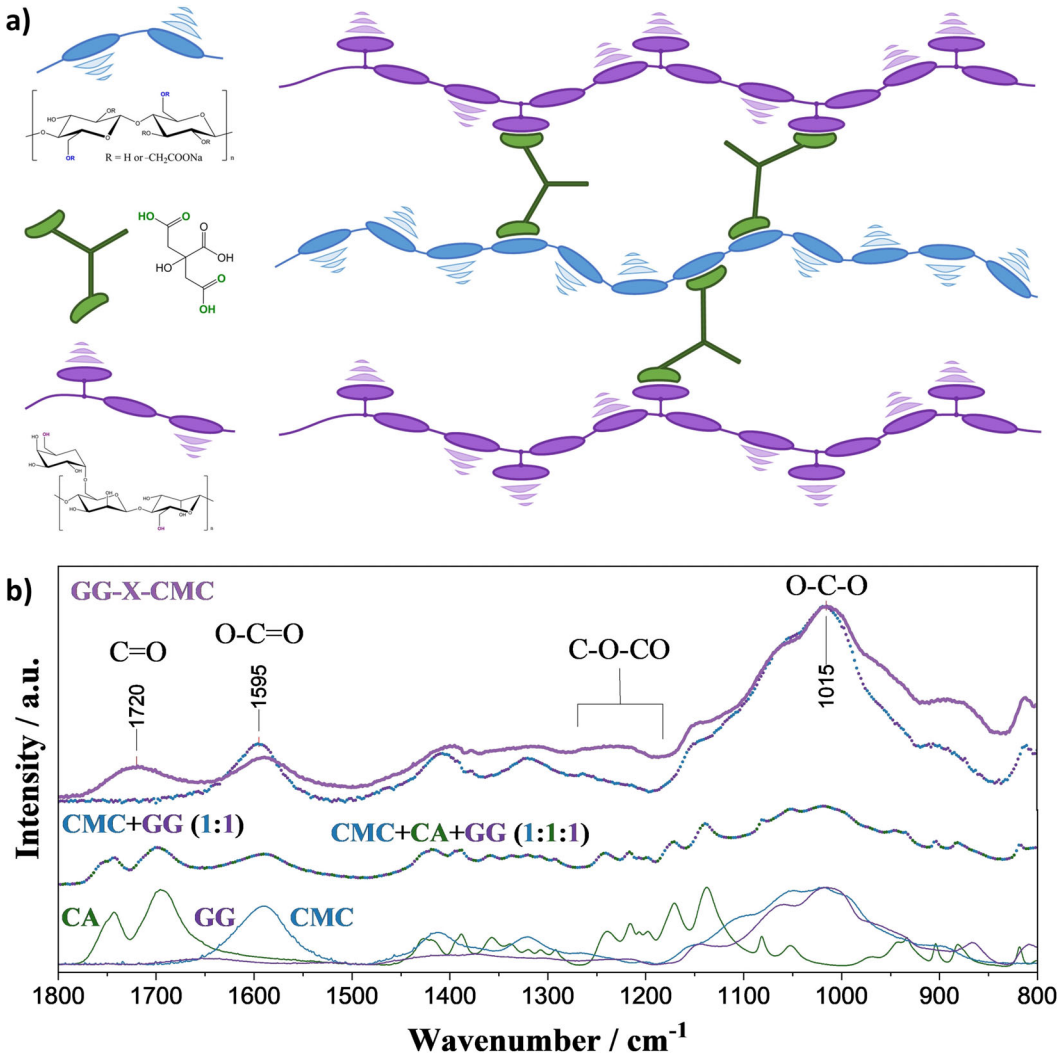

Figure 5. a) Schematic illustration of the co-crosslinked binder network composed of CMC (blue chains) and GG (purple chains) interconnected by CA (green). b) FTIR spectra with the same color code for the single components (CA, GG, and CMC), their mixtures before crosslinking (CMC+GG and CMC+CA+GG) and the co-crosslinked binder (GG–X–CMC, light purple) with the characteristic ester band at $\tilde{\nu} = 1720\ cm^{-1}$.

high-voltage Li-ion cells, CP–GG-3% cathodes (i.e., those that offer the most stable cycling performance) were coupled with graphite anodes, employing CMC as the binder (Figure 7). We employed an optimized electrolyte formulation,[36] and these "green" Li-ion full cells display an excellent cycling stability with 80% capacity retention after 1000 full charge–discharge cycles at 1C (Figure 7a). To our knowledge, this performance exceeds any comparable LNMO|graphite full cell reported so far, especially those that adopt all-water-based electrode-processing strategies.[69–78] A decrease of the charge and discharge rate to C/3 results in slightly higher specific capacities of approximately 110 $mAh\,g^{-1}$, which corresponds to a specific energy of more than 300 $Wh\,kg^{-1}$ based on the cathode and anode active material loading (Figure 7b). The voltage profiles upon cycling show that the cell polarization does not increase notably (Figure 7c). This indicates that the slight capacity loss upon cycling is presumably caused by the loss of lithium or manganese cations from the cathode,[55,56,80] which remains limited thanks to the metal-scavenging properties of the GG binder[44,46,52] and the optimized electrolyte composition.[36]

Conclusions

The replacement of carboxymethyl cellulose (CMC) with guar gum (GG) as a binder for high-voltage $LiNi_{0.5}Mn_{1.5}O_4$ (LNMO) cathodes allows substantially enhanced cycling stabilities at significantly reduced binder contents and the realization of positive electrodes with greatly increased active material mass loadings. GG-based LNMO cathodes with a binder content of 3 wt% outperform CMC-based LNMO cathodes with a binder content of 5 wt% with a capacity retention of approximately 96% compared to approximately 89% after 400 cycles. To tune the rate capability, moreover, the co-crosslinking of both binders through citric acid allows a suitable performance at elevated charge–discharge rates, which depends on the eventual mass loading. Remarkably, GG-based LNMO cathodes coupled with CMC-based graphite anodes provide an excellent cycling

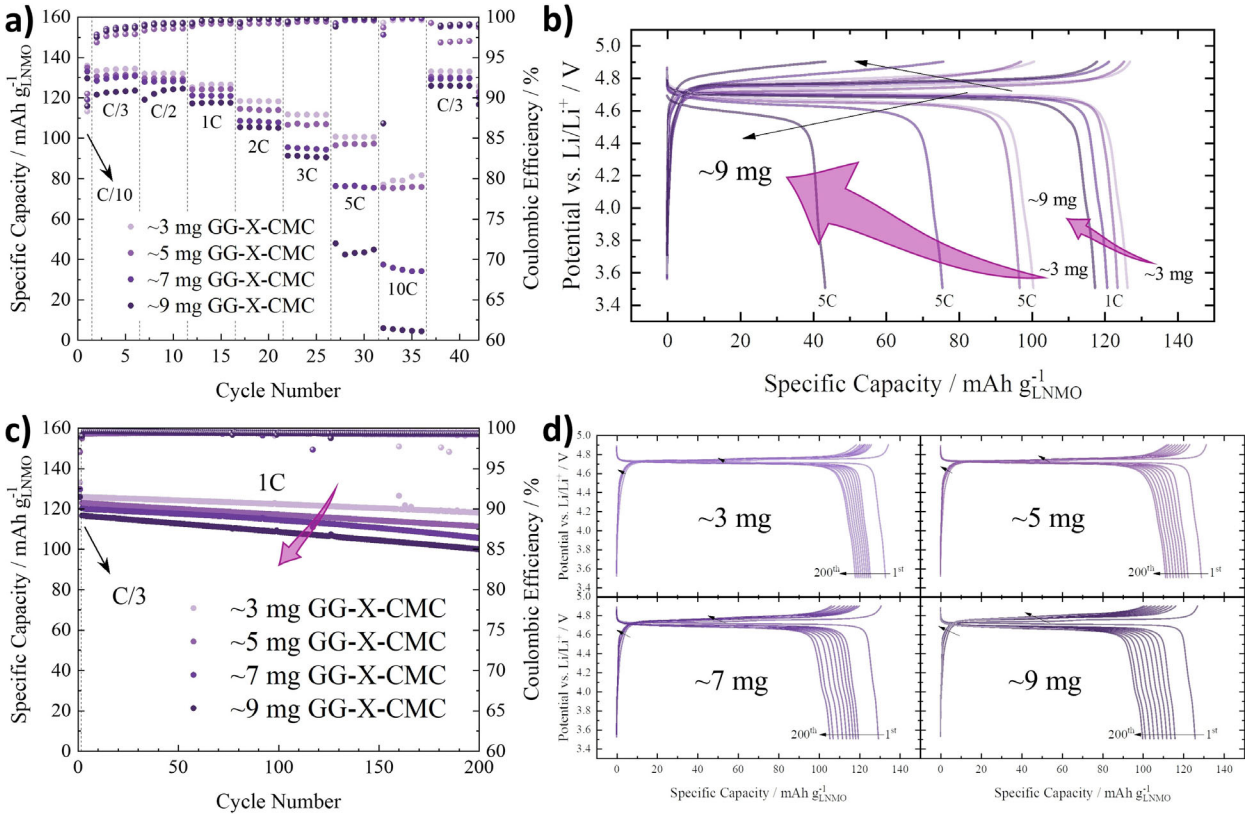

Figure 6. a) Rate capability for GG–X–CMC electrodes with areal loadings of 3 (light purple) to 9 mg cm^{-2} (dark purple) and b) selected potential profiles for these electrodes at 1 and 5 C. c) Constant current cycling and d) selected potential profiles over 200 cycles for the same electrodes. In all cases, the cut-off potentials were set to 3.5 and 4.9 V, and a charge–discharge rate of 1 C corresponds to a specific current of 147 mA g^{-1}.

stability with a capacity retention of 80% after 1000 cycles at 1 C and a promising gravimetric energy density of more than 300 W h kg^{-1} at C/3. Clearly, these results demonstrate the feasibility to employ water-soluble, environmentally friendly biopolymers as a binder for high-voltage LNMO cathodes and, hence, the realization of sustainable and high-performance next-generation lithium-ion batteries.

Experimental Section

Structural and morphological characterization

Pristine $LiNi_{0.5}Mn_{1.5}O_4$ (LNMO; d_{50} = 14.4 μm; BET surface area: < 1.0 m^2 g^{-1}; tap density = 2.26 g cm^{-3}) was synthesized by a continuous co-precipitation method followed by an optimized temperature treatment to tailor the particle size and morphology for high-voltage applications, as reported elsewhere.[81] The material was characterized by using powder XRD by using a Bruker D8 Advance diffractometer ($Cu_{K\alpha}$ radiation, λ = 0.154 nm) in the 2θ range between 10 and 90° and applying a step size of 0.025° with a counting time of 2 s per step. The recorded reflections were analyzed by using the ICDD database, implemented in the EVA software (Bruker). SEM characterization of the cathode tapes was performed by using a Zeiss Crossbeam 340 field-emission electron microscope. FTIR spectra were measured by using a Vertex 70v IR spectrometer (Bruker) equipped with a MIR light source, KBr beam splitter, and a deuterated L-alanine-doped triglycine sulfate (DLaTGS) detector with a KBr window. A single-reflection diamond attenuated total reflection accessory PLATINUM ATR from Bruker was employed for the IR-ATR spectroscopy measurements. The collected spectra were averaged over 64 scans with an optical resolution of 1 cm^{-1}. The elemental composition of the LNMO powder was determined by using inductively coupled plasma optical emission spectrometry (ICP-OES) by using a Spectro Arcos spectrometer (Spectro Analytical Instruments).

Electrode preparation

If not indicated differently, the positive electrode composition was 87 wt% LNMO, 10 wt% conductive carbon (C-ENERGY Super C45, IMERYS), and 3 wt% binder. The latter was either pure sodium carboxymethyl cellulose (CMC; Walocel CRT 2000 GA 07, degree of substitution 0.7, Dow Wolff Cellulosics), natural GG (Lamberti SpA), or a 9:1 mixture of CMC or GG with CA (99%, Sigma–Aldrich). In addition, a 1:1:1 blend of CMC and GG with CA was used. For the electrode preparation, the binder (which included CA) was dissolved in deionized water to obtain a 2.0 wt% solution. If used, PA (orthophosphoric acid 85%, >99%, Bernd Kraft) was added to the binder solution together with the conductive carbon and the active material. The resulting slurry was homogenized by using planetary ball milling for 2 h. The obtained slurry was cast on carbon-coated aluminum foil, which served as the current collector (thickness: 20 μm; battery grade), by using utilizing a laboratory doctor blade (wet film thickness between 200 and 600 μm). After immediate predrying in an atmospheric oven (ED-115, Binder) for 10 min at 80 °C, the electrode tapes were dried at RT overnight in a dry room. Disc electrodes (geometric area: 1.13 cm^2) were punched

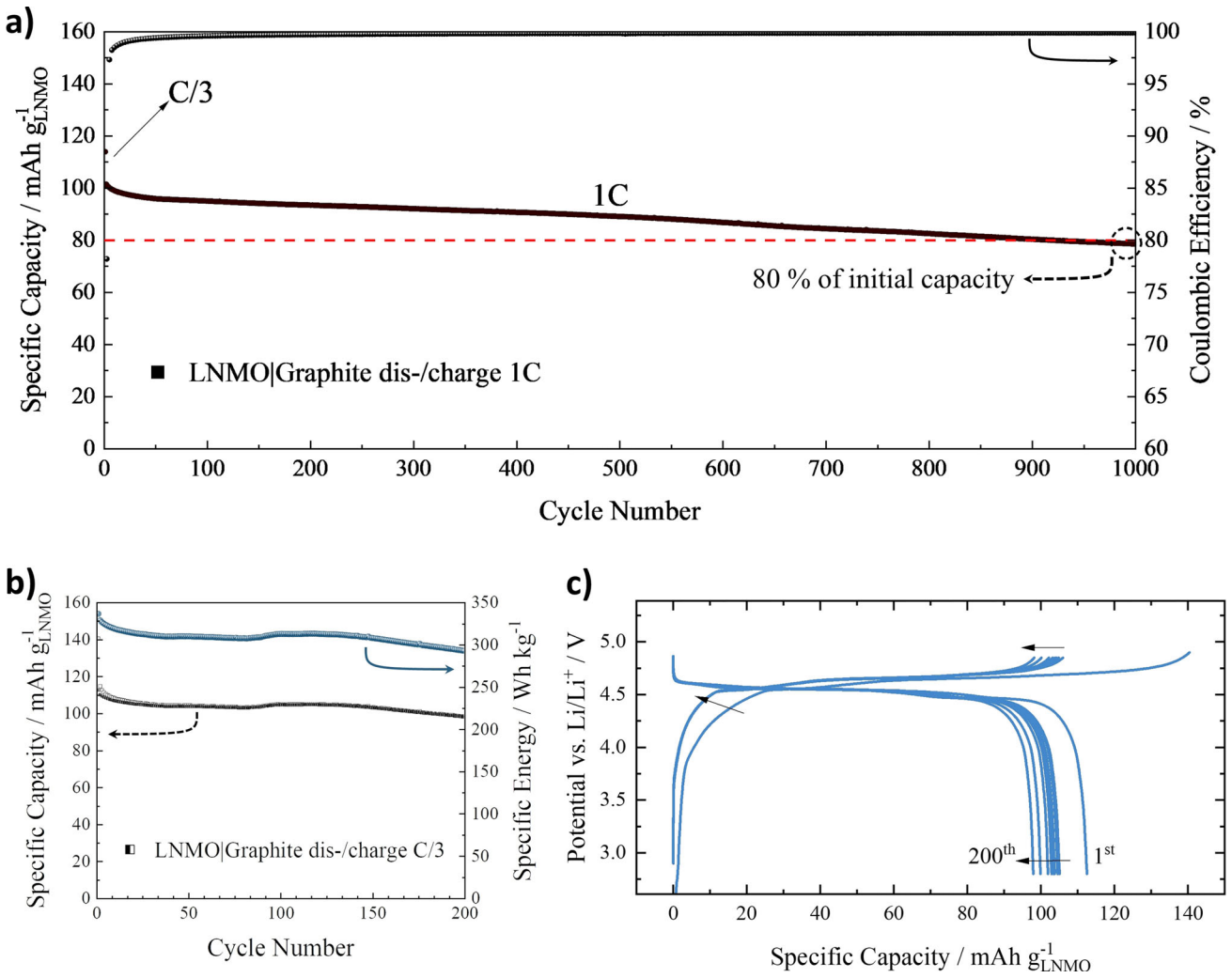

Figure 7. Electrochemical characterization of Li-ion full cells with GG-based LNMO cathodes and CMC-based graphite anodes with an a/c ratio (based on their theoretical capacity) of approximately 1.3. a) Extended constant current cycling at 1 C. b) Constant current cycling at a relatively lower charge–discharge rate of C/3 and the resulting specific energy based on the anode (≈2 mg cm^{-2}) and cathode (≈3.5 mg cm^{-2}) active material masses with c) selected potential profiles for the low-rate cycling. The upper cut-off cell voltage was set to 4.85 V at C/3 and 5.0 V at 1 C, whereas the lower cut-off was fixed at 2.8 V. A charge–discharge rate of 1 C corresponds to a specific current of 147 mA g^{-1}.

and pressed at 5 tons for 1 min (Atlas manual hydraulic press, Specac) under dry atmosphere. Finally, the electrodes were further dried under vacuum at 120 °C for 16 or 14 h at 120 °C and 2 h at 150 °C. The latter procedure was applied if CA was used as a crosslinking agent. If not indicated differently, electrodes with various binders that contain CA for crosslinking had a mass loading in the range of 4.0–4.9 mg cm^{-2} (CMC-based) and 4.3–5.2 mg cm^{-2} (GG-based). Besides, the active material mass loading of the electrodes was adjusted by using different coating thicknesses. For the full cell tests, graphite (SLP30, TIMCAL) anodes were prepared analogously with an electrode composition of 90 wt% SLP30, 5 wt% Super C45, and 5 wt% CMC as binder. The electrode coating thickness was adjusted to reach the desired mass loading for the full cell balancing.

For the FTIR measurements, slurries that contained only water and binder (GG, or its mixture with CMC) were prepared by spreading a 2.0 wt% aqueous solution of the binder on Mylar foil. The coated film was predried at 80 °C before the final drying step at 120 °C.

Electrochemical characterization

Three-electrode Swagelok cells were used for the electrochemical characterization. Lithium metal foils (thickness 500 μm, battery grade, Honjo) served as the counter and reference electrode. The cell was assembled in an Ar-filled glovebox (MB200B ECO, MBraun; H_2O and O_2 content lower than 0.1 ppm) with glass fiber disks (Whatman GF/D) as a separator, soaked in 130 μL of the electrolyte solution [1 M $LiPF_6$ in ethyl carbonate (EC)/dimethyl carbonate (DMC), 1:1 *w/w*, Selectilyte LP 30, BASF]. If not indicated differently, galvanostatic cycling was performed within the potential range of 3.5–4.9 V at (20 ± 2) °C by using a Maccor Battery Tester 4300. The charge-discharge rate of 1 C corresponds to a specific current of 147 mA g^{-1}. All potential and voltage values given herein refer to the Li^+/Li quasi-reference redox couple. For full cell testing, two-electrode coin-cells were used, prepared as described above. The electrodes in the cells were balanced to obtain an A/C ratio of roughly 1.3:1 based on the reversible capacities of the anode (A) and cathode (C), as known from the half-cell tests and, if not indicated differently, cycled in a voltage range of 2.8–4.85 V.

Acknowledgements

The authors would like to acknowledge financial support from the German Federal Ministry of Education and Research within the Li-EcoSafe project (03X4636A & 03X4636D) and from the Helmholtz Association. Furthermore, we are very thankful to Mr. Jakob Asenbauer for performing the ICP measurements.

Conflict of interest

The authors declare no conflict of interest.

Keywords: batteries · energy transfer · lithium · manganese · polymers

[1] H. Ma, F. Balthasar, N. Tait, X. Riera-Palou, A. Harrison, *Energy Policy* **2012**, *44*, 160 – 173.
[2] A. Tovey, "Volvo becomes the first major car manufacturer to go all electric", can be found at https://www.telegraph.co.uk/business/2017/07/05/volvo-becomes-first-major-car-manufacturer-go-electric/, **2017**, accessed March 20, 2019.
[3] P. A. Eisenstein, "GM Is Going All Electric, Will Ditch Gas- and Diesel-Powered Cars", can be found at https://www.nbcnews.com/business/autos/gm-going-all-electric-will-ditch-gas-diesel-powered-cars-n806806, **2017**, accessed March 19, 2019.
[4] C. Hetzner, "BMW exec explains why automaker changed its electrification strategy", can be found at https://europe.autonews.com/automakers/bmw-exec-explains-why-automaker-changed-its-electrification-strategy, **2018**, accessed March 19, 2019.
[5] M. Herdlitschka, C. J. Sedlmayr, K. Groeneveld, "Plans for more than ten different all-electric vehicles by 2022: All systems are go", can be found at https://media.daimler.com/marsMediaSite/en/instance/ko.xhtml?oid=29779739, **2017**, accessed at March 19, 2019.
[6] D. Bresser, K. Hosoi, D. Howell, H. Li, H. Zeisel, K. Amine, S. Passerini, *J. Power Sources* **2018**, *382*, 176 – 178.
[7] B. Scrosati, J. Garche, *J. Power Sources* **2010**, *195*, 2419 – 2430.
[8] D. Larcher, J. M. Tarascon, *Nat. Chem.* **2015**, *7*, 19 – 29.
[9] C. J. Barnhart, S. M. Benson, *Energy Environ. Sci.* **2013**, *6*, 1083.
[10] D. Bresser, D. Buchholz, A. Moretti, A. Varzi, S. Passerini, *Energy Environ. Sci.* **2018**, *11*, 3096 – 3127.
[11] S. Roberts, G. Gunn in *Critical Metals Handbook*, Wiley, **2013**, pp. 122 – 149.
[12] M. Li, J. Lu, Z. Chen, K. Amine, *Adv. Mater.* **2018**, *30*, 1800561.
[13] European Commission, Communication from the Commission to European Parliament, the Council, the European Economic and Social Committee and the Committee of the Regions, **2017**, COM(2017), 8.
[14] United States Department of Energy, **2011**, 190.
[15] I. J. Davidson, S. Niketic, Y. Abu-Lebdeh, F. M. Courtel, D. Duguay, *J. Power Sources* **2010**, *196*, 2128 – 2134.
[16] Y. Nishi, *Chem. Rec.* **2001**, *1*, 406 – 413.
[17] K. P. Lee, N. C. Chromey, R. Culik, J. R. Barnes, P. W. Schneider, *Toxicol. Sci.* **1987**, *9*, 222 – 235.
[18] D. E. Malek, L. A. Malley, T. W. Slone, G. S. Elliott, G. L. Kennedy, W. Mellert, K. Deckardt, C. Gembardt, B. Hildebrand, S. R. Murphy, D. B. Bower, G. A. Wright, *Drug Chem. Toxicol.* **1997**, *20*, 63 – 77.
[19] W. Zhu, D. R. Schmehl, C. A. Mullin, J. L. Frazier, *PLoS One* **2014**, *9*, e77547.
[20] D. L. Wood, J. D. Quass, J. Li, S. Ahmed, D. Ventola, C. Daniel, *Dry Technol.* **2018**, *36*, 234 – 244.
[21] J. L. Li, Z. J. Du, R. E. Ruther, S. J. An, L. A. David, K. Hays, M. Wood, N. D. Phillip, Y. P. Sheng, C. Y. Mao, S. Kalnaus, C. Daniel, D. L. Wood, III, *JOM* **2017**, *69*, 1484 – 1496.
[22] G. Berckmans, M. Messagie, J. Smekens, N. Omar, L. Vanhaverbeke, J. Van Mierlo, *Energies* **2017**, *10*, 1314.
[23] M. Ling, J. Qiu, S. Li, H. Zhao, G. Liu, S. Zhang, *J. Mater. Chem. A* **2013**, *1*, 11543.
[24] H. Buqa, M. Holzapfel, F. Krumeich, C. Veit, P. Novák, *J. Power Sources* **2006**, *161*, 617 – 622.
[25] M. M. Thackeray, M. M. Thackeray, M. M. Thackeray, *J. Am. Ceram. Soc.* **1999**, *82*, 3347 – 3354.
[26] G. E. Brown, V. E. Henrich, W. H. Casey, D. L. Clark, C. Eggleston, A. Felmy, D. W. Goodman, M. Grätzel, G. Maciel, M. I. McCarthy, K. H. Nealson, D. A. Sverjensky, M. F. Toney, J. M. Zachara, *Chem. Rev.* **1999**, *99*, 77 – 174.
[27] I. A. Shkrob, J. A. Gilbert, P. J. Phillips, R. Klie, R. T. Haasch, J. Bareño, D. P. Abraham, *J. Electrochem. Soc.* **2017**, *164*, A1489 – A1498.
[28] H. Yamamoto, H. Mori in *Lithium-Ion Batteries—Science and Technologies*, Springer, **2009**, pp. 163 – 179.
[29] N. Yabuuchi, Y. Kinoshita, K. Misaki, T. Matsuyama, S. Komaba, *J. Electrochem. Soc.* **2015**, *162*, A538 – A544.
[30] N. L. Sukiman, X. Zhou, N. Birbilis, A. E. Hughes, J. M. C. Mol, S. J. Garcia, G. E. Thompson in *Aluminium Alloys—New Trends in Fabrication and Applications*, Intech, **2012**, pp. 47 – 97.
[31] I. Doberdò, N. Löffler, N. Laszczynski, D. Cericola, N. Penazzi, S. Bodoardo, G. T. Kim, S. Passerini, *J. Power Sources* **2014**, *248*, 1000 – 1006.
[32] N. Loeffler, G.-T. T. Kim, F. Mueller, T. Diemant, J.-K. K. Kim, R. J. J. Behm, S. Passerini, *ChemSusChem* **2016**, *9*, 1112 – 1117.
[33] M. Kuenzel, D. Bresser, T. Diemant, D. V. Carvalho, G. T. Kim, R. J. Behm, S. Passerini, *ChemSusChem* **2018**, *11*, 562 – 573.
[34] A. Kazzazi, D. Bresser, A. Birrozzi, J. Von Zamory, M. Hekmatfar, S. Passerini, *ACS Appl. Mater. Interfaces* **2018**, *10*, 17214 – 17222.
[35] Z. Chen, G. Kim, D. Chao, N. Loeffler, M. Copley, J. Lin, Z. Shen, S. Passerini, *J. Power Sources*, **2017**, *372*, 180 – 187.
[36] M. Y. Abeywardana, N. Laszczynski, M. Kuenzel, D. Bresser, S. Passerini, B. Lucht, *Int. J. Electrochem.* **2019**, *2019*, 8636540.
[37] M. Kuenzel, R. Porhiel, D. Bresser, J. Asenbauer, P. Axmann, M. Wohlfahrt-Mehrens, S. Passerini, *Batteries Supercaps* **2020**, *3*, 155 – 164.
[38] M. Kuenzel, D. Bresser, G.-T. Kim, P. Axmann, M. Wohlfahrt-Mehrens, S. Passerini, *ACS Appl. Energy Mater.* **2020**, *3*, 218 – 230.
[39] G. Dodi, D. Hritcu, M. I. Popa, *Cellul. Chem. Technol.* **2011**, *45*, 3 – 4.
[40] T. Hongbo, L. Yanping, S. Min, W. Xiguang, *Polym. J.* **2012**, *44*, 211 – 216.
[41] R. Kuruba, M. K. Datta, K. Damodaran, P. H. Jampani, B. Gattu, P. P. Patel, P. M. Shanthi, S. Damle, P. N. Kumta, *J. Power Sources* **2015**, *298*, 331 – 340.
[42] J. Liu, Q. Zhang, T. Zhang, J. T. Li, L. Huang, S. G. Sun, *Adv. Funct. Mater.* **2015**, *25*, 3599 – 3605.
[43] M. K. Dufficy, S. A. Khan, P. S. Fedkiw, *J. Mater. Chem. A* **2015**, *3*, 12023 – 12030.
[44] J. Liu, Y. Xuan, D. G. D. Galpaya, Y. Gu, Z. Lin, S. Zhang, C. Yan, S. Feng, L. Wang, *J. Mater. Chem. A* **2018**, *6*, 19455 – 19462.
[45] D. V. Carvalho, N. Loeffler, M. Hekmatfar, A. Moretti, G. T. Kim, S. Passerini, *Electrochim. Acta* **2018**, *265*, 89 – 97.
[46] T. Zhang, J. Li, J. Liu, Y. Y. Deng, Z. Wu, Z. Z. Yin, D. Guo, L. Huang, S.-G. Sun, *Chem. Commun.* **2016**, *52*, 4683 – 4686.
[47] B. P. N. Nguyen, S. Chazelle, M. Cerbelaud, W. Porcher, B. Lestriez, *J. Power Sources* **2014**, *262*, 112 – 122.
[48] Z. Karkar, D. Guyomard, L. Roué, B. Lestriez, *Electrochim. Acta* **2017**, *258*, 453 – 466.
[49] W.-J. Cheng, C.-S. Cho, C.-C. Li, *J. Electrochem. Soc.* **2018**, *165*, A2058 – A2060.
[50] B.-R. Lee, S. Kim, E.-S. Oh, *J. Electrochem. Soc.* **2014**, *161*, A2128 – A2132.
[51] Y. N. Sudhakar, M. Selvakumar, D. K. Bhat, *Mater. Sci. Eng. B* **2014**, *180*, 12 – 19.
[52] Y. Q. Lu, J. T. Li, X. X. Peng, T. Zhang, Y. P. Deng, Z. Y. Wu, L. Deng, L. Huang, X. D. Zhou, S. G. Sun, *Electrochem. Commun.* **2016**, *72*, 79 – 82.
[53] Q. Li, H. Yang, L. Xie, J. Yang, Y. Nuli, J. Wang, *Chem. Commun.* **2016**, *52*, 13479 – 13482.
[54] M. H. Ryou, S. Hong, M. Winter, H. Lee, J. W. Choi, *J. Mater. Chem. A* **2013**, *1*, 15224 – 15229.
[55] N. P. W. Pieczonka, Z. Liu, P. Lu, K. L. Olson, J. Moote, B. R. Powell, J.-H. Kim, *J. Phys. Chem. C* **2013**, *117*, 15947 – 15957.
[56] C. Zhan, J. Lu, A. J. Kropf, T. Wu, A. N. Jansen, Y. K. Sun, X. Qiu, K. Amine, *Nat. Commun.* **2013**, *4*, 2437.
[57] B. Aktekin, M. J. Lacey, T. Nordh, R. Younesi, C. Tengstedt, W. Zipprich, D. Brandell, K. Edström, *J. Phys. Chem. C* **2018**, *122*, 11234 – 11248.
[58] T. Marks, S. Trussler, A. J. Smith, D. Xiong, J. R. Dahn, *J. Electrochem. Soc.* **2011**, *158*, A51 – A57.

[59] J. Li, C. Daniel, D. Wood, *J. Power Sources* **2011**, *196*, 2452 – 2460.
[60] D. Mazouzi, Z. Karkar, C. R. Hernandez, P. J. Manero, D. Guyomard, L. Roué, B. Lestriez, *J. Power Sources* **2015**, *280*, 533 – 549.
[61] B. Koo, H. Kim, Y. Cho, K. T. Lee, N. S. Choi, J. Cho, *Angew. Chem. Int. Ed.* **2012**, *51*, 8762 – 8767; *Angew. Chem.* **2012**, *124*, 8892 – 8897.
[62] J. Song, M. Zhou, R. Yi, T. Xu, M. L. Gordin, D. Tang, Z. Yu, M. Regula, D. Wang, *Adv. Funct. Mater.* **2014**, *24*, 5904 – 5910.
[63] R. M. Silverstein, F. X. Webster, D. Kiemle, *Spectrometric Identification of Organic Compounds, 7th ed.*, Wiley, **2005**.
[64] Y. A. Arfat, M. Ejaz, H. Jacob, J. Ahmed, *Carbohydr. Polym.* **2017**, *157*, 65 – 71.
[65] D. Mudgil, S. Barak, B. S. Khatkar, *Int. J. Biol. Macromol.* **2012**, *50*, 1035 – 1039.
[66] J. Čopíková, M. Černá, M. Novotná, J. Kaasová, A. Synytsya, *Czech J. Food Sci.* **2001**, *19*, 51 – 56.
[67] D. L. Wood, J. Li, C. Daniel, *J. Power Sources* **2015**, *275*, 234 – 242.
[68] A. Kwade, W. Haselrieder, R. Leithoff, A. Modlinger, F. Dietrich, K. Droeder, *Nat. Energy* **2018**, *3*, 290 – 300.
[69] N. P. W. Pieczonka, V. Borgel, B. Ziv, N. Leifer, V. Dargel, D. Aurbach, J. H. Kim, Z. Liu, X. Huang, S. A. Krachkovskiy, G. R. Goward, I. Halalay, B. R. Powell, A. Manthiram, *Adv. Energy Mater.* **2015**, *5*, 1501008.
[70] F. De Giorgio, N. Laszczynski, J. von Zamory, M. Mastragostino, C. Arbizzani, S. Passerini, *ChemSusChem* **2017**, *10*, 379 – 386.
[71] L. Xue, K. Ueno, S. Y. Lee, C. A. Angell, *J. Power Sources* **2014**, *262*, 123 – 128.
[72] T. J. Lee, J. Soon, S. Chae, J. H. Ryu, S. M. Oh, *ACS Appl. Mater. Interfaces* **2019**, *11*, 11306 – 11316.
[73] M. S. Milien, H. Beyer, W. Beichel, P. Klose, H. A. Gasteiger, B. L. Lucht, I. Krossing, *J. Electrochem. Soc.* **2018**, *165*, A2569 – A2576.
[74] S. Solchenbach, M. Wetjen, D. Pritzl, K. U. Schwenke, H. A. Gasteiger, *J. Electrochem. Soc.* **2018**, *165*, A512 – A524.
[75] G. Gabrielli, P. Axmann, T. Diemant, R. J. Behm, M. Wohlfahrt-Mehrens, *ChemSusChem* **2016**, *9*, 1670 – 1679.
[76] J. C. Fang, Y. F. Xu, G. L. Xu, S. Y. Shen, J. T. Li, L. Huang, S. G. Sun, *J. Power Sources* **2016**, *304*, 15 – 23.
[77] L. Hu, K. Amine, Z. Zhang, *Electrochem. Commun.* **2014**, *44*, 34 – 37.
[78] L. Hu, Z. Xue, K. Amine, Z. Zhang, *J. Electrochem. Soc.* **2014**, *161*, A1777 – A1781.
[79] J. H. Kim, N. P. W. Pieczonka, P. Lu, Z. Liu, R. Qiao, W. Yang, M. M. Tessema, Y. K. Sun, B. R. Powell, *Adv. Mater. Interfaces* **2015**, *2*, 1500109.
[80] J. H. Kim, N. P. W. Pieczonka, Z. Li, Y. Wu, S. Harris, B. R. Powell, *Electrochim. Acta* **2013**, *90*, 556 – 562.
[81] P. Axmann, G. Gabrielli, M. Wohlfahrt-Mehrens, *J. Power Sources* **2016**, *301*, 151 – 159.

Manuscript received: December 19, 2019
Revised manuscript received: February 28, 2020
Accepted manuscript online: March 3, 2020
Version of record online: ■■ ■■, 0000

FULL PAPERS

M. Kuenzel, H. Choi, F. Wu, A. Kazzazi, P. Axmann, M. Wohlfahrt-Mehrens, D. Bresser,* S. Passerini*

■■ – ■■

Co-Crosslinked Water-Soluble Biopolymers as a Binder for High-Voltage $LiNi_{0.5}Mn_{1.5}O_4$ | Graphite Lithium-Ion Full Cells

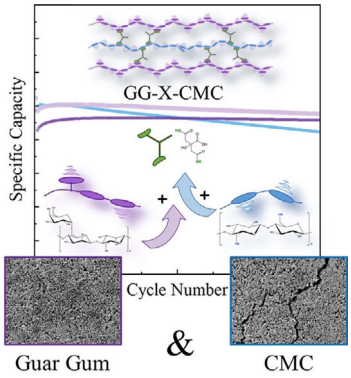

Great gum: The use of crosslinked guar gum as a binder for high-voltage $LiNi_{0.5}Mn_{1.5}O_4$ allows increased mass loadings, decreased binder contents, and enhanced cycling stability with a capacity retention of 80% after 1000 cycles in $LiNi_{0.5}Mn_{1.5}O_4$ | graphite full cells. Co-crosslinking with carboxymethyl cellulose further improves the rate capability to render the aqueous electrode preparation a viable option for commercial applications.